Applied Physics Letters

The stress-strain relationship of liquid marbles under compression

Cite as: Appl. Phys. Lett. **114**, 043701 (2019); https://doi.org/10.1063/1.5079438
Submitted: 31 October 2018 . Accepted: 05 December 2018 . Published Online: 28 January 2019

Hasitha-Nayanajith Polwaththe-Gallage, Chin Hong Ooi, Jing Jin, Emilie Sauret, Nam-Trung Nguyen, Zirui Li, and YuanTong Gu

AIP Publishing

Applied Physics Letters ARTICLE scitation.org/journal/apl

The stress-strain relationship of liquid marbles under compression

Cite as: Appl. Phys. Lett. **114**, 043701 (2019); doi: 10.1063/1.5079438
Submitted: 31 October 2018 · Accepted: 5 December 2018 · Published Online: 28 January 2019

Hasitha-Nayanajith Polwaththe-Gallage,[1] Chin Hong Ooi,[2] Jing Jin,[2] Emilie Sauret,[1,a)] Nam-Trung Nguyen,[2,a)] Zirui Li,[3] and YuanTong Gu[1,a)]

AFFILIATIONS

[1] School of Chemistry, Physics and Mechanical Engineering, Faculty of Science and Engineering, Queensland University of Technology, 2-George Street, Brisbane, QLD 4001, Australia
[2] Queensland Micro- and Nanotechnology Centre, Griffith University, 170 Kessels Road, 4111 Queensland, Australia
[3] Institute of Laser and Optoelectronic Intelligent Manufacturing, Wenzhou University, Wenzhou 325035, People's Republic of China

[a)] **Authors to whom correspondence should be addressed**: emilie.sauret@qut.edu.au; nam-trung.nguyen@griffith.edu.au; and yuantong.gu@qut.edu.au

ABSTRACT

Liquid marbles can be characterized using elastic solid models consisting of a liquid surrounded by a soft solid membrane. The elastic properties of liquid marbles determine the amount of compression under a given external force. This is an important property as the elasticity of liquid marbles determines their morphology under a given stress. We show that the stress-strain relationship of liquid marbles can be described by $\sigma^* \mathrm{Bo} = 0.6[1/(1-\varepsilon_{hro})^2 - 1]$, where Bo is the Bond number, σ^* is the normalised stress, and ε_{hr0} is the strain measured with respect to the equivalent radius of the liquid marble. This stress-strain relationship could pave the way for the development of microfluidic devices with robust liquid marbles.

Liquid marbles are classified as non-wetting liquid droplets with the characteristics of soft solids. As there is no direct physical contact between the liquid interior and the surroundings, liquid marbles are capable of virtually lossless transport of small liquid volumes. Their low cost and ease of preparation make liquid marbles highly desirable instruments in digital microfluidics.[1]

Research on the elasticity of liquid marbles has been steadily gaining attention in the research arena, and this includes the controllable deformation of liquid marbles coated with monolayer nanoparticles.[2–4] The rationale behind such works could be that the survivability of a liquid marble heavily depends on its elasticity. Furthermore, it is important to note that large deformations of liquid marbles may lead to substantial internal mixing which is conducive to cell viability, a critical aspect in using liquid marbles as bio-reactors. The simple parallel plate compression test was usually conducted with the goal of comprehending the robustness of liquid marbles.[5–7] This well-established method has been used to investigate the properties of liquids,[8] solids,[9] and gels.[10] Asare-Asher *et al.* investigated the Young's modulus of a liquid marble and reported its non-linear elastic characteristics.[6] Whyman and Bormashenko determined the surface tension of liquid marbles under compression by applying some geometrical assumptions.[11] Rendos *et al.* also investigated the surface tension of liquid marbles under compression, albeit using the energy conservation approach.[5] Liu *et al.* characterised the robustness of a liquid marble by quantifying the surface coverage of the coating particles.[7] In principle, the combination of a liquid interior and a thin coating necessitates a more comprehensive model than a model that uses a single-phase. Also, liquid marble coatings consist of loose powder that cracks readily, which could render the membrane encapsulated liquid model unsuitable. As such, the development of a universal model is motivated by this prevailing challenge. The developed model aims to describe the elasticity of a liquid marble with more rigour without resorting to geometric assumptions. Also, the development of the universal stress-strain relationship for liquid marbles can be fundamental in designing microfluidic devices with robust liquid marbles.

In this study, we investigate the elasticity of a liquid marble using a large-strain, parallel plate compression test with high resolution. To obtain large strains whilst maintaining the integrity of the liquid marble, the plates have been coated with the same hydrophobic powder as the marble. A coarse grained liquid marble model[12] is employed to obtain the stress-strain

relationship of a 10 μl water droplet coated with polytetrafluoroethylene (PTFE) particles. After validating the liquid marble model against the experimental results, the model is used to evaluate the effect of the volume of the droplet, the density, and the surface tension of the liquid on the stress-strain relationship of the liquid marbles. Then, the model predictions are used to develop a generalised stress-strain relationship applicable to any liquid marble. Finally, the validity of the generalised equation is assessed using the experimental results.

Liquid marbles were prepared using the well-known droplet rolling on the powder bed method. Using a micropipette (Thermo Scientific Finnpipette 4500, 0.5–10 μl), a small liquid droplet is dispensed onto a powder bed of polytetrafluoroethylene (PTFE, Sigma-Aldrich® 1 μm nominal diameter) and rolled around until the droplet is fully coated. The liquid droplet consists of deionized (DI) water (MilliQ® Direct 8 system, 18 MΩ·cm) infused with fluorescein sodium salt (Sigma-Aldrich® F6377) at 0.25 g/l to facilitate the image analysis.

Two glass slides were coated with PTFE. The first glass slide was placed on the weighing pan of the electronic balance (RADWAG AS82/220.R2), which acts as the bottom slide with the powdered side facing up. The second glass slide was attached to a vertically mounted linear stage (Zaber Technologies T-LS28M), which acts as the top slide with the powdered side facing down. The two slides were positioned in the weighing chamber of an electronic balance. The camera was mounted on another set of linear stages for fine-focusing and placed adjacent to the electronic balance.

Subsequently, a liquid marble was placed on the bottom slide and the electronic balance was zeroed. The linear stage was programmed to move downwards at a speed of 5 μm/s to fulfil the quasi-static condition. The magnitude of the downward stroke was approximately 0.7 h_0, with h_0 being the uncompressed height of the sessile marble. The top slide was programmed to compress the marble and then for 10 s at maximum compression before returning to its initial position at the same speed. The linear stage was started simultaneously with the image and weight data acquisition. The data pertaining to the weight were sampled at the maximum rate of the electronic balance corresponding to 2 frames per second (fps). The colour camera recorded the compression process at the same rate.

The side view of liquid marbles was acquired using a colour USB camera (Edmund Optics) with telecentric lenses at 0.3, 0.5, and 0.1× magnification. The image resolution was kept at 800 × 600 pixels for all the experimental tests [Figs. 1(a) and 1(b)]. The image data were analysed using MATLAB, MathWorks [Figs. 1(c)–1(e)]. The image analysis procedure is as follows: (i) apply colour threshold to generate a binary image of the liquid marble, (ii) de-noise and measure the box width and the height of the liquid marble, and (iii) repeat preceding steps for every frame. Figure 1 (Multimedia view) shows compression of a 10 μl liquid marble. From Fig. 1 (Multimedia view), the liquid marble does not fully recover to its initial shape after removing the load. This could be attributed to the interfacial jamming which results from increased local coating particle density during retraction.[13]

This study employs the same numerical model we previously developed to predict the morphological behaviour of magnetic

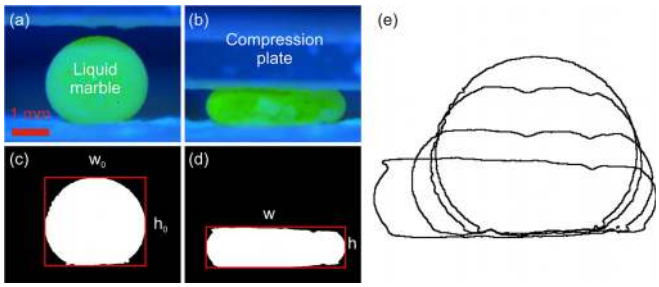

FIG. 1. Side views of a 10-μl liquid marble under compression and its corresponding analysed images. (a) Liquid marble in position prior to compression. (b) Liquid marble in compression, shown with the compression plate. (c) Analysed image with the initial box width and height shown. (d) Analysed image with the box width and height shown. (e) Outlines of the liquid marble at different compression stages overlaid against each other. Multimedia view: https://doi.org/10.1063/1.5079438.1

liquid marbles.[12] However, the model is further improved to replicate the exact experimental setup and to avoid the initiation of cracks on the liquid marble. The force acting on the fluid particles due to the hydrostatic pressure $\mathbf{F}^g$ (Fig. 2) is defined as

$$\mathbf{F}^g = h_h \rho g l_0 \delta z, \tag{1}$$

where h_h is the height from the top most point of the liquid droplet to the particle of interest, ρ is the density of the liquid, g is the acceleration of the gravity, l_0 is the current mean distance between two consecutive liquid particles, and δz is the thickness of the liquid particles, which is used to calculate the area of the particle.[12] Similar to our previous work,[12] δz is set to 0.1 mm. The force acting on the fluid particles due to the surface tension is given by

$$\mathbf{F}^s = \frac{\gamma}{r} l_0 \delta z, \tag{2}$$

where γ is the surface tension of the liquid and r is the radius of curvature at the particle of interest. The Lennard-Jones (LJ) type forces are used to model the interaction forces ($\mathbf{F}^{ss}$) between solid particles, given by

$$\mathbf{F}^{ss} = \frac{f_0^{ss}}{r^{ss}} \left[\left(\frac{r_0^{ss}}{r^{ss}} \right)^{13} - \left(\frac{r_0^{ss}}{r^{ss}} \right)^{7} \right], \tag{3}$$

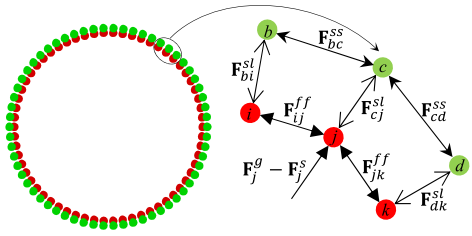

FIG. 2. Initial particle representation (green particles—PTTE coating and red particles—surface of the liquid droplet) of the liquid marble and the forces acting on the particles; $\mathbf{F}^{sl}$: the interaction forces between solid and liquid particles, $\mathbf{F}^{ss}$: the interaction forces between consecutive solid particles, $\mathbf{F}^{ff}$: the interaction forces between consecutive liquid particles, $\mathbf{F}^{g}$: the forces acting on the fluid particles due to the hydrostatic pressure, and $\mathbf{F}^{s}$: the forces acting on the fluid particles due to the surface tension.

where f_0^{ss} is the strength of the LJ contact for the solid-solid interaction, r^{ss} is the present distance between two consecutive solid particles, and r_0^{ss} is the original distance between two consecutive solid particles. However, in this improved model, only the repulsive forces between solid particles are considered (when $r^{ss} < r_0^{ss}$), which leads to the increase in the number of solid particles in the event the distance between the consecutive solid particles increases. Therefore, the improved model replicates the exact experimental setup. The interaction between liquid particles is modelled by

$$\mathbf{F}^{ff} = k_l \frac{\partial}{2\partial \mathbf{r}} \left(\frac{l - l_0}{l_0} \right)^2, \tag{4}$$

where k_l is the energy constant for the liquid-liquid interaction, $\mathbf{r}$ is the position vector of the particle, and l is the present length between two consecutive liquid particles. The interaction between solid and liquid particles ($\mathbf{F}^{sl}$) and the conservation of the volume of the liquid droplet are modelled by the same formulations as in the previous model.[12] In addition, all the simulation parameters including l_0, f_0^{ss}, r_0^{ss}, and k_l are assigned as described in the previous work.[12]

A horizontal plate is used to compress the liquid marble in this model which is moved down until the liquid marble is compressed up to the intended amount (Δh). Then, the horizontal boundary is kept at that level, and the simulations are run further until the whole system reaches a steady state (in terms of dimensions and forces). According to Figs. 3(a)–3(d), the compressed shapes of the liquid marble are closely align with the experimental results in Fig. 1. The sum of all the y-components of the forces acting on the particles at the top boundary (ΣF_t) and the sum of all the y-components of the forces acting on the particles at the bottom boundary (ΣF_b) are calculated separately [Fig. 3(e)]. Initially, the simulations are conducted for a liquid marble of 10 μl, and the results are compared against the experimental data.

The compressive stress on the liquid marble is calculated from the experiments, defined by

$$\sigma_1 = \frac{4F_1}{\pi w_0^2}, \tag{5}$$

where σ_1 is the compressive stress, F_1 is the measured applied force, and w_0 is the width of the uncompressed marble [Fig. 3(e)]. The compressive stress on the liquid marble is calculated from the numerical simulations and has the form

$$\sigma_1 = \frac{\Sigma F_t}{w_0 \delta z}. \tag{6}$$

The strain of the liquid marble is calculated in terms of change in the height (h_0-h)

$$\varepsilon_h = \frac{h_0 - h}{h_0}. \tag{7}$$

According to Fig. 4(a), the stress-strain curve obtained from the numerical model aligns well with the experimental results obtained from three repeated experimental tests. Overall, the stress on the liquid marble shows a polynomial increase with the strain of the liquid marble. The volume of the liquid droplet coated with PTFE particles was modified in order to investigate the effect of the volume of the liquid droplet on the stress-strain behaviour of the liquid marbles. The density (ρ) and surface tension (γ) of the liquid are set to 997 kg/m^3 and 0.072 N/m, respectively, while all the other parameters are left intact. As shown in Fig. 4(b), for a given ε_h, σ_1 decreases with the volume of the liquid marble. This phenomenon could be explained by the radius of the curvature of the liquid marbles. The two liquid marbles with two different volumes (i.e., 15 μl and 50 μl) have the same strain, as shown in insets in Fig. 4(b). However, the smaller liquid marble (i.e., 15 μl) has a smaller total radius of curvature compared to the 50 μl liquid marble. Therefore, the force induced on the smaller liquid marble, due to the Young-Laplace pressure, $p^s = \gamma(1/r_1 + 1/r_2)$, is higher compared to the larger liquid

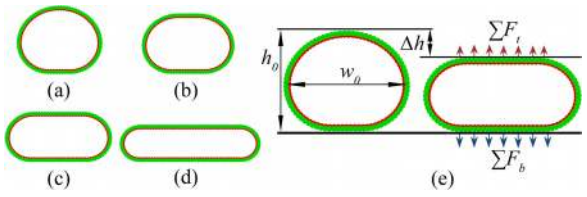

FIG. 3. Simulated compressed shapes of the liquid marble of 10 μl at ε_h = (a) 0, (b) 0.11, (c) 0.32, (d) 0.51, and (e) the compressed shape of the liquid marble when the liquid marble is compressed by Δh.

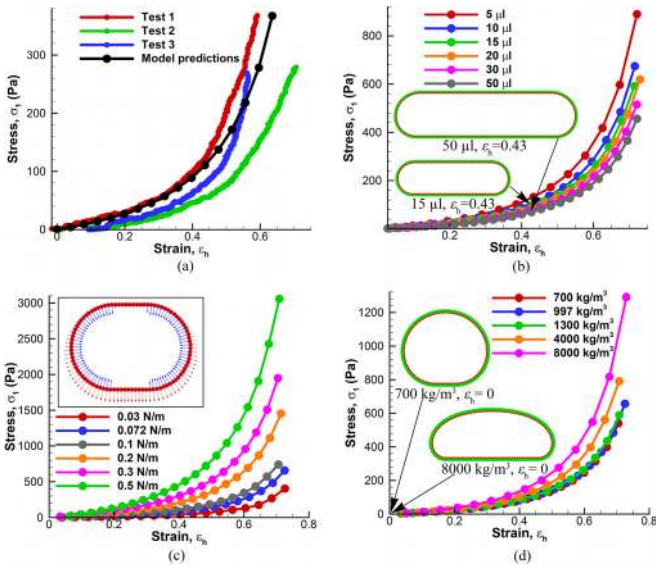

FIG. 4. (a) Comparison of the stress-strain curves (σ_1 vs. ε_h) of the three repeated experimental tests of the 10 μl liquid marble and numerical simulations. (b) Variation of σ_1 vs. ε_h obtained from the numerical model, for different volumes of the liquid marbles; insets show that the smaller liquid marble has a smaller radius of curvature compared to the larger liquid marble. (c) Variation of σ_1 vs. ε_h obtained from the numerical model for different surface tensions of liquid; the inset shows the direction of Young-Laplace pressure forces (blue arrows) and hydrostatic pressure forces (red arrows). (d) Variation of σ_1 vs. ε_h obtained from the numerical model for different densities of liquid; insets shows the shapes of two liquid marbles with ρ = 700 kg/m^3 and 8000 kg/m^3 at rest.

marble (herein, r_1 and r_2 are the principal radii of curvatures). This p^S resists the compression of the liquid marble, and consequently, for a given ε_h, σ_1 decreases with the volume of the liquid marble.

The effect of the surface tension of the liquid on the stress-strain behaviour of the liquid marbles is investigated by varying the surface tension of a 15 μl liquid droplet coated with PTFE particles. The density of the liquid is set to 997 kg/m^3. As can be seen in Fig. 4(c), for a given ε_h, σ_1 increases with the surface tension of the liquid. The rise in σ_1 with the surface tension of the liquid can be explained again by the pressure p^s. When the surface tension increases, p^s increases and resists the compression of the liquid marble because p^s acts in the inward normal direction to the surface of the liquid droplet. Therefore, for a given ε_h, σ_1 increases with the surface tension of the liquid.

The same liquid marble is employed to investigate the effect of the density of the liquid on its stress-strain behaviour by varying the density of the liquid, while the surface tension of the liquid is set to 0.072 N/m. According to Fig. 4(d), for a given ε_h, σ_1 gradually increases with the density of the liquid. However, this rise in σ_1 is insignificant compared to that change in σ_1 with the surface tension of the liquid. However, the liquid density does not resist the compression of the liquid marble. In fact, when the density of the liquid is higher, the uncompressed liquid marbles exhibit puddle-like shapes [Fig. 4(d), inset] and infers a somewhat a self-induced compression. This self-induced hydrostatic pressure acts in the outward normal direction to the surface of the liquid droplet and can be calculated by $p^g = h_h \rho g$ (where h_h is the height from the top most point of the liquid droplet to the point at which the hydrostatic pressure is required to be calculated and g is the acceleration of gravity). Therefore, it is clear that the liquid density assists in the compression of the liquid marble. However, this contradicts with the results shown in Fig. 4(d). The main reason for this contradiction stems from the difference in the initial uncompressed width (w_0) and height (h_0) of two liquid marbles [Fig. 4(d), insets], even though they have the same volume. Therefore, we should use an appropriate and practical approach to calculate and compare the stress-strain behaviour of liquid marbles.

We emphasized that the conventional stress-strain analysis is not suitable to accurately calculate and compare the stress-strain behaviour of liquid marbles. Therefore, an alternative approach needs to be used. In this regard, a liquid marble with a nearly spherical shape ($\varepsilon_{hr0} \approx 0$) at rest [Fig. 5(b)] is considered. Then, the forces acting on the liquid marble are analysed, and the analytical solution is derived to explain the stress-strain relationship of the liquid marbles as described below.

The strain of the liquid marble can be calculated with respect to the radius of the un-deformed liquid marble is given by

$$\varepsilon_{hr0} = \frac{2r_0 - h}{2r_0}, \tag{8}$$

where r_0 is the radius of the un-deformed liquid marble [Fig. 5(a)], which is calculated by $r_0 = (3V/4\pi)^{1/3}$, and V is the volume of the liquid marble. The stress acting on the liquid marble at rest can be calculated by using its weight and its original equivalent radius r_0

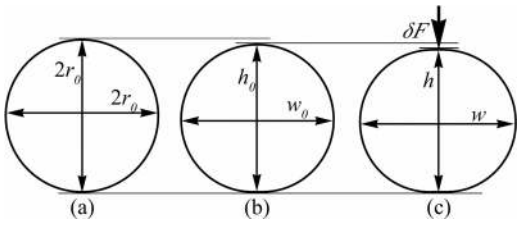

FIG. 5. (a) The equivalent undeformed shape of the liquid marble, (b) the uncompressed shape of the liquid marble at rest, and (c) the compressed shape of the liquid marble by an external force, δF.

$$\sigma_0 = \frac{4r_0\rho g}{3}, \tag{9}$$

when a small external force (δF) is applied on the liquid marble, assuming that its height changes from h_0 to h and its width changes from w_0 to w [Figs. 5(b) and 5(c)]. At this stage, the stress acting on the liquid marble is given by

$$\sigma_2 = \frac{4F_2}{\pi w_0^2}, \tag{10}$$

where $F_2 = \delta F + 4\pi r_0^3 \rho g/3$, and

$$\frac{\sigma_2}{\sigma_0} = \left(\frac{r_0^2}{w_0^2}\right)\frac{3F_2}{\pi r_0^3 \rho g}. \tag{11}$$

It has been analytically, experimentally, and numerically proven[12] that the height of a liquid marble at rest can be obtained as follows:

$$h = 2r_0 \quad \text{if Bo} \ll 1, \tag{12a}$$

$$h = 2r_0 \text{Bo}^{-1/2} \quad \text{if Bo} \gg 1. \tag{12b}$$

It is noteworthy that Bo is the Bond number, $\text{Bo} = \rho g r_0^2/\gamma$, which illustrates the dominance of the gravitational energy over the surface energy of the liquid marbles. Generally, when Bo $\ll$ 1, liquid marbles exhibit spherical shapes. However, when a liquid marble is compressed by an external force, it does not show a spherical shape; instead, the liquid marble exhibits a puddle-like shape. Therefore, the height of the liquid marble can be assumed by $h = 2r_0\text{Bo}_{\text{new}}^{-1/2}$. However, Bo_{new} should be calculated by considering the total force acting on the liquid marble. However, it is noteworthy that δF is not distributed over the whole volume of the liquid marble as δF is applied only on the top contact area of the liquid marble. Therefore, we should use correction factors in order to obtain the accurate effect from the external force

$$\text{Bo}_{new} = C_1\frac{3F_2}{4\pi r_0\gamma} + C_2. \tag{13}$$

Here, C_1 and C_2 are the correction factors. Therefore, from Eqs. (8), (12b), and (13)

$$C_1\frac{3F_2}{4\pi r_0\gamma} + C_2 = \frac{1}{(1-\varepsilon_{hr0})^2}. \tag{14}$$

Finally, from Eqs. (11) and (14)

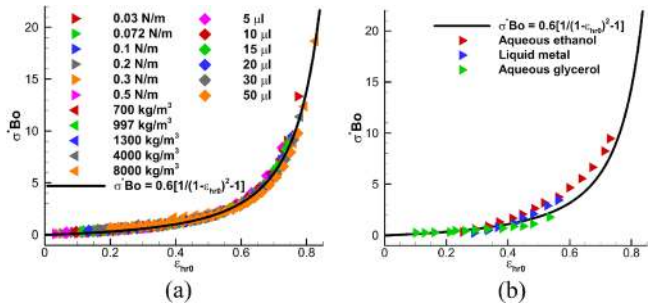

FIG. 6. (a) The variation of σ^*Bo against ε_{hr0}, calculated from Figs. 4(b)–4(d). (b) Variation of σ^*Bo against ε_{hr0} for aqueous ethanol (25% volume), liquid metal (Pure eutectic Ga-In), and aqueous glycerol (50% volume), compared to the proposed equation.

$$\frac{C_1 r_0^2 \rho g}{\gamma}\left(\frac{\sigma_2}{\sigma_0}\right)\left(\frac{w_0}{2r_0}\right)^2 = \frac{1}{(1-\varepsilon_{hr0})^2} - C_2. \tag{15}$$

Since $w_0 \approx 2r_0$ and $\mathrm{Bo} = r_0^2\rho g/\gamma$

$$\left(\frac{\sigma_2}{\sigma_0}\right)\mathrm{Bo} = \frac{1}{(1-\varepsilon_{hr0})^2}\left(\frac{1}{C_1}\right) - \left(\frac{C_2}{C_1}\right). \tag{16}$$

In theory, if ε_{hr0} is zero, the liquid marbles should exhibit a pure spherical shape, and this happens if and only if Bo is zero. These conditions are fulfilled only when $1/C_1$ is equal to C_2/C_1. Therefore, finally, we can define this relationship as

$$\left(\frac{\sigma_2}{\sigma_0}\right)\mathrm{Bo} = C_3\left[\frac{1}{(1-\varepsilon_{hr0})^2} - 1\right], \tag{17}$$

where C_3 is a constant and σ_2/σ_0 can be defined as the normalised stress (σ^*) acting on the liquid marble. σ_2 is the stress induced on the liquid marble during the compression due to the total force acting on the liquid marble, and σ_0 is the stress induced on the liquid marble before it is compressed due to the self-weight of the liquid marble. Here, C_3 is the only unknown, and the liquid marble model predictions for the stress-strain relationships of liquid marbles can be used to estimate C_3.

σ_2 and σ_0 can be numerically calculated as follows:

$$\sigma_2 = \frac{\Sigma F_b}{w_0 \delta z}, \tag{18}$$

$$\sigma_0 = \frac{\Sigma F_b}{2r_0 \delta z}, \tag{19}$$

where abs $(\Sigma F_b) = \mathrm{abs}(\Sigma F_t) + F_w$, with F_w being the total weight of the liquid marble (i.e., the weight of the liquid droplet and PTFE coating). This is a more practical approach to analyse the stress-strain behaviour of liquid marbles since it considers the total force including the weight of the liquid marble itself, acting on the liquid marble. According to Fig. 6, $\sigma*$ Bo shows a polynomial increase with ε_{hr0}, and for a given ε_{hr0}, $\sigma*$ Bo takes a unique value regardless of the density, surface tension, or the volume of the liquid droplet. Using MATLAB curve fitting tools, we found that $\sigma * \mathrm{Bo} = 0.6[1/(1-\varepsilon_{hr0})^2 - 1]$.

In order to examine the validity of this equation, further experiments are carried out to obtain the stress-strain curves of liquid marbles with three different liquids: aqueous ethanol (25% volume, $\rho = 947\,\mathrm{kg/m^3}$, and $\gamma = 0.039\,\mathrm{N/m}$[14]), liquid metal (Pure eutectic Ga-In, $\rho = 6250\,\mathrm{kg/m^3}$, and $\gamma = 0.329 \pm 0.169$ N/m), and aqueous glycerol (50% volume, $\rho = 1131\,\mathrm{kg/m^3}$, and $\gamma = 0.068\,\mathrm{N/m}$[15]), and they are compared with the developed equation. In this experiment, the volume of each liquid marble is fixed at 10 μl. The surface tension values of aqueous ethanol and glycerol were obtained from the literature,[14,15] whereas the surface tension of eutectic Ga-In was calculated based on the measured side profile and its known density.

The experimental results comply with the proposed equation, as shown in Fig. 6(b). In conclusion, the relationship $\sigma * \mathrm{Bo} = 0.6[1/(1-\varepsilon_{hr0})^2 - 1]$ is not only valid for liquid marbles of pure water but also valid for any other liquid marbles of various liquids with different fluid properties, namely, density and surface tension. Importantly, this stress-strain relationship can be used in designing microfluidic devices with liquid marbles.

We thank the Queensland Micro- and Nanotechnology Centre for providing the facilities to make the experiments possible, and the support provided by the High Performance Computer (HPC) resources in the Queensland University of Technology (QUT) is gratefully acknowledged. The Australian Research Council (ARC) is thanked for its financial support under Grant Nos. ARC-DECRA DE130101183, LP150100737, DP150100828, and DP170100277. The authors gratefully acknowledge the proofreading of the manuscript and the valuable comments provided by Sahan T. W. Kuruneru of the Queensland University of Technology.

REFERENCES

[1]N.-T. Nguyen, M. Hejazian, C. Ooi, and N. Kashaninejad, Micromachines **8**, 186 (2017).
[2]X. Li, Y. Xue, P. Lv, H. Lin, F. Du, Y. Hu, J. Shen, and H. Duan, Soft Matter **12**, 1655 (2016).
[3]X. Li, Y. Wang, J. Huang, Y. Yang, R. Wang, X. Geng, and D. Zang, Appl. Phys. Lett. **111**, 261604 (2017).
[4]X. Li, R. Wang, H. Shi, and B. Song, Appl. Phys. Lett. **113**, 101602 (2018).
[5]A. Rendos, N. Alsharif, B. L. Kim, and K. A. Brown, Soft Matter **13**, 8903 (2017).
[6]S. Asare-Asher, J. N. Connor, and R. Sedev, J. Colloid Interface Sci. **449**, 341 (2015).
[7]Z. Liu, X. Fu, B. P. Binks, and H. C. Shum, Langmuir **31**, 11236 (2015).
[8]C. Norotte, F. Marga, A. Neagu, I. Kosztin, and G. Forgacs, EPL **81**, 46003 (2008).
[9]Y.-L. Lin, D.-M. Wang, W.-M. Lu, Y.-S. Lin, and K.-L. Tung, Chem. Eng. Sci. **63**, 195 (2008).
[10]R. D. Egholm, S. F. Christensen, and P. Szabo, J. Appl. Polym. Sci. **102**, 3037 (2006).
[11]G. Whyman and E. Bormashenko, J. Colloid Interface Sci. **457**, 148 (2015).
[12]H.-N. Polwaththe-Gallage, E. Sauret, N.-T. Nguyen, S. C. Saha, and Y. Gu, Phys. Fluids **30**, 017105 (2018).
[13]X. Li, Y. Wang, Y. Yang, S. Wang, D. Zang, and X. Geng, Appl. Phys. Lett. **113**, 133702 (2018).
[14]G. Vazquez, E. Alvarez, and J. M. Navaza, J. Chem. Eng. Data **40**, 611 (1995).
[15]Glycerine Producers' Association, *Physical Properties of Glycerine and its Solutions* (Glycerine Producers' Association, 1963).